Tracking Atrial Fibrillation Mechanisms: a Computational Method for Locating Rotors and Ectopic Activity Using Curl and Divergence Operators

Italo Sandoval[1], John A Sims[1], João Salinet[1]

[1] Federal University of ABC, São Bernardo do Campo, Brazil

Abstract

Atrial Fibrillation (AF) is the most common supraventricular arrhythmia and has different underlying activation mechanism, including functional rotors (FR) and ectopic foci (EF). In this work we propose an approach for locating FR and EF in potential maps, which were tested with mathematical phantoms. 12 phantoms were created (128x128 array, 4 s, Fs 500 Hz), simulating the motion of: FR (4 maps), EF (4 maps) and superpositions of these (4 maps). These were downsampled to different grids from 16x16 to 8x8, simulating electrode acquisition. Noise (SNR from 2 to 60) was added. To locate the mechanism, the signals were filtered and interpolated. Farneback optical flow was applied to compute the motion vector field (MVF). The MVF was normalized and its temporal average was calculated. Finally, we computed curl and divergence, by using a x and y oriented 11×11 *Sobel filter as a estimation of the of the partial derivatives. The location of extrema in the curl and divergence maps were used for locating FR and EF respectively. Method robustness was tested by comparing the algorithm performance on different grid sizes and SNR. The mechanism was considered to be detected accurately if the position was within a normalized error of 5% from its respective phantom location. The results showed that our approach was able to locate both mechanisms, but revealed a dependency on spatial resolution.*

1. Introduction

Atrial Fibrillation (AF) is the most common supraventricular arrhythmia and has different underlying activation mechanism, including functional rotors (FR) and ectopic foci (EF) [1, 2]. AF is also associated with an increased morbidity related to heart failure and ictus [2–4]. FR consist of functional reentrant activity where the curved wavefront and wavetail meet each other at a singularity point, or phase singularity, a point where all phase values converge [5–7]. As demonstrated in experiments with isolated hearts and supported by animal and patient studies, self-sustained FR can be present in the atria, leading to complex patterns of activation, possibly being the source of paroxysmal and chronic AF [8]. EF describes a condition where a set of cells depolarize in a independent rhythm that fires spontaneously, creating a wave that spread radially [1, 9].

1.1. Optical Flow

Optical flow (OF) is the apparent motion of brightness patterns in an image sequence. Sparse OF provides a vector field for special features, normally pixels corresponding to edges or corners of objects, while dense OF provides a vector field for all pixels in the image. Dense algorithms related to motion vector field (MVF) analysis are known to have medical imaging applications, in particular for temporal analysis of cardiac images [4, 10–13]. A number of different methods exist for quantification of OF [14–16] of which the dense OF algorithms by Horn and Schunck (HS) and Farneback (FOF) have been used extensively in the literature.

Furthermore, there are various ways to detect FR and EF and the proposed methods could use techniques based on phase analysis, local activation time, or OF.

Ríos-Muñoz et al. (2018) used signals acquired from patients with persistent AF and *in silico* simulations to validate an approach using activation time maps [4]. Firstly the signal was approximated by a linear function obtained by minimizing the mean square error, and the activation was detected from the function slope. For the *in silico* models, the authors deployed a squared 16×16 node grid, emulating 256 different electrodes recording. After the transform, the signal was interpolated using Shepard's method [4, 17]. Ríos-Muñoz and others used OF from the isochronal maps, estimated by HS [4, 15]. For locating rotational activity, the authors applied convolution to the MVF with a kernel containing a rotational pattern. Bellmann et al. (2018) also used OF, applied to transformed signals, with HS method [12, 15]. In this study, OF was also used to identify FR and EF, and compare the located mechanisms before and after surgical intervention. Roney et al. (2021) used OF from maps of normalized filtered derivatives of signals to

study preferential pathways in AF patient and models [13]. These authors also used HS for OF estimation. OF was used to construct a streamline visualization that, in turn, was used to perform qualitative analyses of FR and EF, among other analyses [13].

As can be seen, several studies have applied HS to the analysis of cardiac potential maps, which could be due to its computational efficiency and ease of implementation. Despite this, alternative methods exist for dense OF quantification, including Farneback's OF, which is a newer and more capable method than HS [18], and was used in this work.

FOF is a motion estimation algorithm based on a polynomial expansion transform [16]. With this algorithm the motion is calculated for every pixel, generating a bidimensional MVF for every pair of consecutive frames. The neighborhood of each pixel is approximated by a quadratic polynomial expansion given by Equation 1 [16]:

$$f(x) = x^T Ax + b^T x + c \tag{1}$$

where A is a symmetric matrix, b is a vector and c a scalar. These values are obtained by the weighted least square method, with the weight value decreasing radially from the center, and the neighborhood size is an arbitrary parameter. The displacement d is estimated by considering the polynomial expansion for the second frame $f_2(x)$ the polynomial expansion for the first frame after went through a translation $f_1(x-d)$, showing that the translation d can be found by solving the Equation 2:

$$d = -\frac{1}{2}A_1^{-1}(b_2 - b_1) \tag{2}$$

In this work, we propose and validate a method to detect two FA mechanisms by using FOF and MVF analysis, and distinguish EF and FR, and also clockwise and counterclockwise FR.

2. Methods

Figure 1 illustrates our pipeline for location of EF and FR mechanisms using FOF to compute the MVF and then estimating the operators curl and divergence. The methodology was validated using mathematical phantoms. The phantoms were also used for parameter tuning and assessing algorithm robustness.

2.1. Phantom Creation

12 phantoms were created (128x128 grid with 2000 time samples at $500Hz$), simulating EF (4 phantoms), FR (4 phantoms) and superposition of both mechanisms (4 phantoms, see supplementary material [19]). Equation 3 summarizes the EF phantom (P_{EF}) creation. The EF phantoms were created by: (i) determine the position (i_0, j_0) of the mechanism center; (ii) compute the Euclidean distance from each pixel, with position (i, j), to the mechanism center, then multiplied by an arbitrary coefficient A related to spatial propagation of the signals; (iii) for each time instant, add a temporal increment $I(t)$ to the map values, related to the sampling frequency (fs) and the mechanism's underlying activation frequency (F); and (iv) these values were used in a reverse sawtooth function, truncated to the 4th order of its respective Fourier series $SAW(x)$, used as a simple approximation of the activation potential.

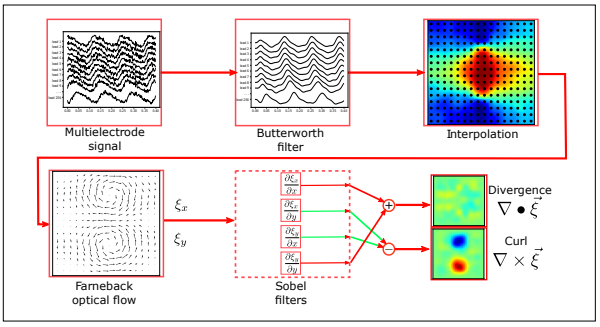

Figure 1. Pipeline for the mechanism location approach.

$$\begin{aligned} P_{EF}(i,j,t) &= SAW(A||\vec{v}|| + I(t)) \\ \vec{v} &= (i - i_0,\ j - j0) \\ I(t) &= \frac{t}{2fsF\pi} \\ SAW(x) &= -\sum_{n=1}^{4} \frac{1}{n} sin(xn) \end{aligned} \tag{3}$$

Equation 4 summarizes the creation of the FR phantom (P_{FR}). The FR phantom was created by: (i) selecting two positions (i_0, j_0) and (i_1, j_1) for the mechanism: one clockwise and another counter-clockwise; (ii) two phase maps Ph_0 and Ph_1 were created by calculating the relative angle from each pixel to the mechanism position; (iii) the angle θ, referring to the relative mechanism positions, was subtracted from Ph_0 and added to Ph_1, aligning the maps; (iv) the maps were multiplied by a weight, w, summed, then a temporal increment $I(t)$ was added to these values; and finally (v) the combined phase maps were used in a reverse sawtooth function $SAW(x)$ as previously described.

$$\begin{aligned} P_{FR}(i,j,t) &= SAW(Ph_0 w + Ph_1(1-w) + I(t)) \\ Ph_0 &= atan2(j - j_0, i - i_0) - \theta \\ Ph_1 &= -atan2(j - j_1, i - i_1) - \pi + \theta \\ \theta &= atan2(j_0 - j_1, i_0 - i_1) \\ \vec{v} &= (i - i_0,\ j - j0),\ \ \vec{v}_1 = (i_1 - i_0,\ j_1 - j_0) \\ w &= min\left(max\left(comp_{\vec{v}_1}\vec{v},\ 0\right),\ 1\right) \end{aligned} \tag{4}$$

Here, $atan2(a, b)$ is a function similar to $tan^{-1}(a/b)$, but considers the sign of a and b separately so as to produce a domain from $-\pi$ to $+\pi$ instead of $-\pi/2$ to $+\pi/2$).

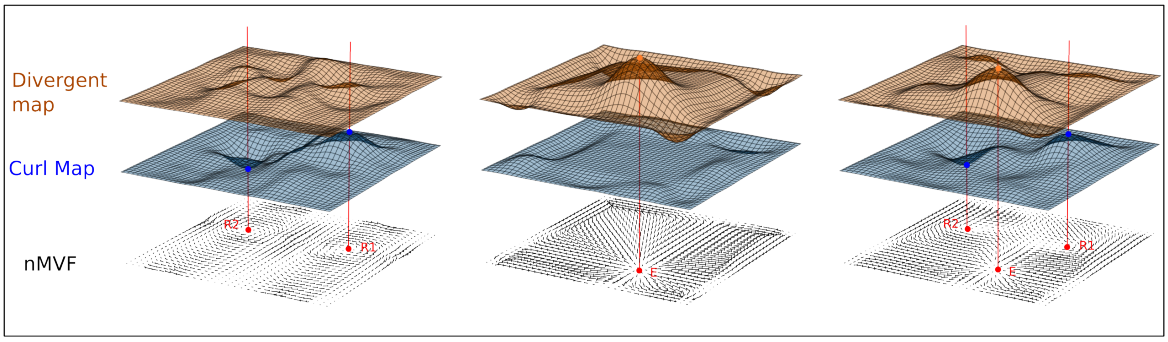

Figure 2. Divergent and curl maps and nMVF for three different phantoms (FR, a EF and a superposition, respectively), for a 16x16 grid with SNR 60. The blue dots represents FR position in the curl maps and orange dots represents EF position in the divergent maps.

To simulate electrode acquisition, the phantom signals were sampled in grids from 8x8 to 16x16, and noise with SNR from 60 to 2 was applied to the signals to evaluate the method's robustness to noise degradation.

2.2. Determination of mechanism location

Figure 1 shows the main steps for our mechanism location approach. Initially, the signals are filtered with a Butterworth bandpass filter, then interpolated with cubic splines. Next, the FOF algorithm, available in the OpenCV library (v.4.5.4) for Python 3, is used, being applied to each pair of consecutive time samples, obtaining the MVF. This is normalized and its temporal average calculated (nMVF), a process that decreases random artifact components and amplifies persistent patterns, as performed in other works [4, 12]. The curl and divergent potential maps were obtained by: (i) Approximating the partial derivatives in x and y directions. Sobel filters of size of 11×11 pixels were applied to each component of the nMVF, respectively $nMVF_x$ and $nMVF_y$, providing the estimates of $\frac{\partial(nMVF_x)}{\partial x}$, $\frac{\partial(nMVF_y)}{\partial x}$, $\frac{\partial(nMVF_x)}{\partial y}$, $\frac{\partial(nMVF_y)}{\partial y}$. (ii) Next, curl and divergent maps were obtained using Equations 5 and 6:

$$\texttt{Div.Map} = \frac{\partial(nMVF_x)}{\partial x} + \frac{\partial(nMVF_y)}{\partial y} \quad (5)$$

$$\texttt{Curl Map} = \frac{\partial(nMVF_y)}{\partial x} - \frac{\partial(nMVF_x)}{\partial y} \quad (6)$$

(iii) The mechanisms were detected and located in the curl and divergent maps by applying a threshold to the curl and divergent maps, then calculating the center of each region with value above the threshold. The mechanisms detected from the curl maps are FR and from the divergent maps EF. (iv) The method accuracy was measured by considering as true positive a detection with normalized error below 5%.

3. Results and discussion

Figure 2 show the obtained nMVF, curl and divergent maps for a FR, a EF and a superposition phantom, respectively, and on a 16x16 grid with SNR 60. As expected, FR appear as extrema in the curl maps, with its sign showing the direction of rotation. In the same way, EF appears as maxima in the divergent maps. The divergence operator shows higher absolute values where there is no conservation of energy. Considering the electrophysiology of the cardiomyocytes, the energy would be *generated* when a localized set of activated cells trigger a larger number of cells, increasing the signal intensity. This would lead to a maximum divergence when the set of cells activates all the surroundings, which is the nature of an EF.

Table 1. Location accuracy of the algorithm for different levels of SNR and acquisition grids.

		Grid			
	SNR	16x16	12x12	10x10	8x8
P_{FR}	60	1.000	0.717	0.708	0.633
	20	1.000	0.717	0.875	0.646
	10	1.000	0.725	0.875	0.667
	5	1.000	0.750	1.000	0.708
	2	1.000	0.625	1.000	0.375
P_{EF}	60	1.000	1.000	1.000	0.000
	20	1.000	1.000	1.000	0.000
	10	1.000	1.000	1.000	0.000
	5	1.000	1.000	1.000	0.000
	2	1.000	1.000	0.250	0.000
Sup.	60	1.000	0.917	0.542	0.417
	20	1.000	0.917	0.542	0.417
	10	1.000	0.875	0.583	0.417
	5	1.000	0.875	0.667	0.500
	2	0.750	0.250	0.000	0.000

Table 1 shows the results for the analysis of accuracy

for the various phantoms. In the FR phantom, with 10×10 and 8×8 grid, the accuracy did not have a maximum value in the higher SNR, which was verified to be due to false positives that disappear as the noise increases. The curl value at the FR location had high variance as the grid and SNR changes, which made it difficult to set a value for the threshold, as this value should be the same for all tests.

It is possible to see a sharp decrease in accuracy from the 10×10 to 8×8 grid, for the EF phantoms. This decrease was more linear for the other phantoms. Therefore, the results show reasonable noise robustness, for all SNR values for the FR phantoms, and at least up to SNR 5 for the others. However, results were dependent on the spatial resolution of the maps. Qualitatively, the curl and divergent maps seems to be highly correlated with the mechanisms, perhaps improved processing of these maps could lead to a more precise location.

4. Conclusions

In this preliminary study, we proposed an approach based on optical flow and vector field operators for locating, and therefore tracking, two of the main AF mechanisms. Our results showed that the approach was successful in locating the mechanisms, including ectopic foci, even in low spatial resolution and SNR conditions.

Acknowledgments

I. Sandoval is supported by Coordenação de Aperfeiçoamento de Pessoal de Nível Superior - Brasil (CAPES). J. Salinet and J. Sims are supported by grant #2018/25606-2, São Paulo Research foundation (FAPESP).

References

[1] Page RL, Joglar JA, Caldwell MA, et al. 2015 ACC/AHA/HRS guideline for the management of adult patients with supraventricular tachycardia: a report of the american college of cardiology/american heart association task force on clinical practice guidelines and the heart rhythm society. J Am Coll Cardiol 2016;67(13):e27–e115.

[2] Zipes DP, Jalife J, Stevenson WG. Cardiac Electrophysiology: From Cell to Bedside. Philadelphia, PA, EUA: Elsevier, 2018.

[3] Wakili R, Voigt N, Kääb S, et al. Recent advances in the molecular pathophysiology of atrial fibrillation. J Clin Invest Aug 2011;121:2955–3968.

[4] Ríos-Muñoz GR, Arenal A, Artés-Rodríguez A. Real-time rotational activity detection in atrial fibrillation. Front Physiol Mar 2018;9.

[5] Pandit SV, Jalife J. Rotors and the dynamics of cardiac fibrillation. Circulation Research 2013;112(5):849–862.

[6] Vijayakumar R, Vasireddi S, Cuculich P, et al. Methodology considerations in phase mapping of human cardiac arrhythmias. Circ Arrhythm Electrophysiol 2016;9:e004409.

[7] Marques VG, Rodrigo M, Guillem MS, et al. Characterization of atrial arrhythmias in body surface potential mapping: A computational study. Comput Biol Med 2020; 127(103904).

[8] Jalife J, Berenfeld O, Mansour M. Mother rotors and fibrillatory conduction: a mechanism of atrial fibrillation. Cardiovascular research May 2002;54(2):204–216.

[9] Marriott HJL, Conover MH. Advanced Concepts in Arrhythmias. St. Louis, Toronto: The C. V. Mosby Company, 1983.

[10] Guo Q, Mandal MK, Liu G, et al. Cardiac video analysis using hodge–helmholtz field decomposition. Comput Biol Med 2006;36(1):1–20.

[11] Sims JA, Giorgi MC, Oliveira MA, et al. Directional analysis of cardiac motion field from gated fluorodeoxyglucose pet images using the discrete helmholtz hodge decomposition. Comput Med Imaging Graph 2018;65:69–78. Advances in Biomedical Image Processing.

[12] Bellmann B, Lin T, Ruppersberg P, et al. Identification of active atrial fibrillation sources and their discrimination from passive rotors using electrographical flow mapping. Clin Res Cardiol Nov 2018;107:1021–1032.

[13] Roney CH, Child N, Porter B, et al. Time-averaged wavefront analysis demonstrates preferential pathways of atrial fibrillation, predicting pulmonary vein isolation acute response. Front Physiol Set 2021;12.

[14] Ogle KN. The perception of the visual world. James. Cambridge, Massachusetts, EUA: Koughton Mifflin Company: Boston, 1951.

[15] Horn BKP, Schunck BG. Determining optical flow. Artificial Intelligence 1981;17(1-3):185–203.

[16] Farnebäck G. Two-frame motion estimation based on polynomial expansion. In Bigun J, Gustavsson T (eds.), Image Analysis. Berlin, Heidelberg: Springer Berlin Heidelberg, 2003; 363–370.

[17] Shepard D. A two-dimensional interpolation function for irregularly-spaced data. In Proceedings of the 1968 23rd ACM National Conference. New York, NY, USA: Association for Computing Machinery, 1968; 517–524.

[18] Nemadea NA, Gohokarb VV. Comparative performance analysis of optical flow algorithms for anomaly detection. Proceedings of International Conference on Communication and Information Processing ICCIP 2019 May 2019;.

[19] Supplementary materials at https://github.com/heartlab-ufabc/electrophysiology/tree/main/characterization/tracking-atrial-fibrillation-mechanisms-a-computational-method-for-locating-rotors-and-ectopic-activity-using-curl-and-divergence-operators-supplementary-materials.

Address for correspondence:

Italo Sandoval Ramos de Oliveira
Alameda da Universidade, s/n, Bairro Anchieta, São Bernardo do Campo - SP, Brazil
italo.sandoval@ufabc.edu.br